

Impact of collisions on the dust wake potential with Maxwellian and non-Maxwellian ions

Sita Sundar, Hanno Kählert, Jan-Philip Joost, Patrick Ludwig, and Michael Bonitz¹

Institut für Theoretische Physik und Astrophysik, Christian-Albrechts-Universität zu Kiel, Leibnizstrasse 15, Kiel 24098, Germany

This work examines the formation of wake fields caused by ions streaming around a charged dust particle, using three-dimensional particle-in-cell (PIC) simulations with charge-neutral collisions included. The influence of an external driving electric field, which leads to a non-Maxwellian distribution of ions, is investigated in detail. The wake features formed for non-Maxwellian ions exhibit significant deviations from those observed within the model of a shifted Maxwellian distribution. The dependence of the peak amplitude and position of the wake potential upon the degree of collisionality is analyzed for a wide range of streaming velocities (Mach numbers). In contrast to a shifted Maxwellian distribution of ions, the drift-driven non-Maxwellian distribution exhibits an increase of the wake amplitude of the first attractive peak with increase in collisionality for high streaming velocities. At very low Mach numbers, collision-induced amplification is observed for Maxwellian as well as non-Maxwellian distributions.

I. INTRODUCTION

Complex (or dusty) plasmas constitute a well-studied^{1–4} interdisciplinary research area. Due to the presence of micron-sized, highly charged dust particles in addition to electrons, ions and neutrals, these plasmas are endowed with features like self-organization and crystal-structures⁵, low-frequency waves (dust acoustic modes)⁶, or the formation of dust-free structures (voids) in micro-gravity experiments⁷. Complex plasmas have close connections with astrophysics (e.g., dust in planetary rings or cometary tails), low-temperature gas discharge operation (dust inserted into or grown in-situ in gas discharges)⁸, fusion related research (dust generated in plasma-surface interactions)^{9–11}, warm-dense matter (strong coupling physics)^{12,13} as well as the broad regime of material sciences (e.g., defects or wave propagation in dust crystals)^{14,15}.

When a dust particle is inserted into a low-temperature plasma, its potential is screened by the electrons and ions. In the sheath region of gas discharges, where the dust typically levitates, strong electric fields and significant ion flows occur. It has been established^{16,17} that the deflection of streaming ions in the electric field of the dust particle leads to quasi-periodic waveforms downstream of the grain. In the linear response (LR) formalism, e.g.^{16,18,19}, the wake potential is linearly proportional to the grain charge, Q_d . Winske *et al.*¹⁷, however, found a nonlinear relationship between charge and wake potential utilizing one- and two-dimensional PIC-simulations. Hutchinson *et al.*²⁰ also reported the nonlinear suppression of the peak potential in the oscillatory wake structure and a reasonable agreement with linear response calculations in the linear regime.

Kinetic models that study the effect of streaming ions on a system of dust particles often adopt a distribution function that is a shifted Maxwellian. However, Lampe *et al.*²² have calculated the steady state distribution function $f(\vec{v})$ for ions subject to ion-neutral charge-exchange collisions in the presence of an electric field, using Monte-

Carlo simulations, and obtained a non-Maxwellian distribution²². Their result is quite distinct from the shifted Maxwellian distribution. The physical characteristics of the non-Maxwellian distribution are due to the presence of collisions and the force field that gives rise to the ion drift. This modified distribution has been shown to influence the ion drag on the grain^{23,24}, the ion-dust streaming instability²⁵, and also affects profoundly the physics of wake formation^{26–28}. While Maxwellian ions give rise to several potential minima and maxima downstream of the grain²⁹, non-Maxwellian ions usually exhibit only one pronounced maximum²⁶. However, a detailed and systematic numerical analysis of non-Maxwellian effects on the nonlinear wake potential is still missing.

Therefore, in this work, we provide such an analysis. In particular, we present a wide-ranging numerical exploration of the role of charge-exchange collisions and the ion distribution function on the wake formation around a grain in a uniform streaming plasma using the three-dimensional Particle-in-Cell (PIC) simulation code COPTIC²⁰. In contrast to linear response calculations^{27,28}, this allows us to fully account for nonlinear effects, which are expected to play an important role in the close vicinity of the grain. We calculate the wake potential for various conditions and study the effect of the distribution function on the wake formation. One of the most interesting results is that *collisions do not necessarily weaken or destroy wake effects*, as is usually expected. In contrast, we report that *charge-exchange collisions may even enhance wake effects*, and we present an explanation for this observation.

The outline of the paper is as follows. In Sec. II, we present a brief description of the distribution functions and their physical interpretation. This is followed by details of the three-dimensional particle-in-cell simulations (COPTIC), in Sec. III. In Sec. IV, we discuss the topology of the potential, the influence of the ion distribution function (Maxwellian versus non-Maxwellian), and present systematic results (comparison of peak heights, peak positions) for a broad range of plasma parameters, including a wide range of Mach numbers and collision

frequencies. Finally, we present a summary and our conclusions in Sec. V.

II. ION DISTRIBUTION FUNCTION

The simple choice of a *shifted Maxwellian distribution* is often a good description of streaming effects without external fields and without any significant effect of collisions. However, in the sheath region of discharges, the ions undergo collisions with the neutrals and experience a strong acceleration towards the electrodes by the sheath electric field. This has been shown to affect their distribution function considerably¹⁶. Even the inclusion of a small degree of collisionality and a (uniform) external field (mean electric field) affect the distribution. The main difference, compared to a shifted Maxwellian with the same drift velocity, is that the self-consistently calculated distribution retains a considerable fraction of low-velocity ions. These distributions have been named *drift-driven distributions* (non-Maxwellian distributions). The nomenclature of *shifted Maxwellian distribution* and *drift-driven distribution* that has been adopted in Ref.²⁶ will be used throughout this paper. The form of the self-consistent background distribution depends on the source of the ion drift and the type of collisions incorporated.

In the picture of the *shifted Maxwellian distribution*, the drift velocity of the neutral particles is the same as that of the ions. There is no external electric field explicitly taken into account, and the ion flow is driven by the neutral flow. As a result, the shifted ion distribution and the neutral distribution are identical, which also implies that their temperatures are equal, $T_i = T_n$. Hence, after a collision, the new ion has a net (neutral) flow velocity. In contrast, in the case of the *drift-driven distribution*, the drift velocity of neutrals is zero, and the ion flow is driven by the external electric field. Thus, ion-neutral charge-exchange collisions give rise to ions with zero drift velocity upon collision, see also Ref.²⁶.

For cases where the contribution of ion-ion collisions is smaller than that of ion-neutral charge exchange collision (i.e. for low degree of ionization), the drift solution of the Boltzmann equation with a BGK-collision term (relaxation time approximation with constant ion-neutral collision frequency ν_{in}) in the presence of a uniform external driving field E_0 can be delineated analytically as²²

$$f_z(u_z) = \frac{1}{2M_{th}} \exp\left(\frac{1 - 2M_{th}u_z}{2M_{th}^2}\right) \times \left[1 + \operatorname{erf}\left(\frac{M_{th}u_z - 1}{\sqrt{2}M_{th}}\right)\right]. \quad (1)$$

Here, $u_z = v_z/v_{th}$ denotes the velocity in the streaming direction (normalized to the thermal velocity of neutrals, v_{th}), and $M_{th} = v_d/v_{th}$ the thermal Mach number, where $v_d = qE_0/(m\nu_{in})$ is the drift velocity (ion charge q). The ion Mach number M can now be defined in terms of the thermal Mach number M_{th} as $M = v_d/c_s = \sqrt{T_i/T_e} M_{th}$,

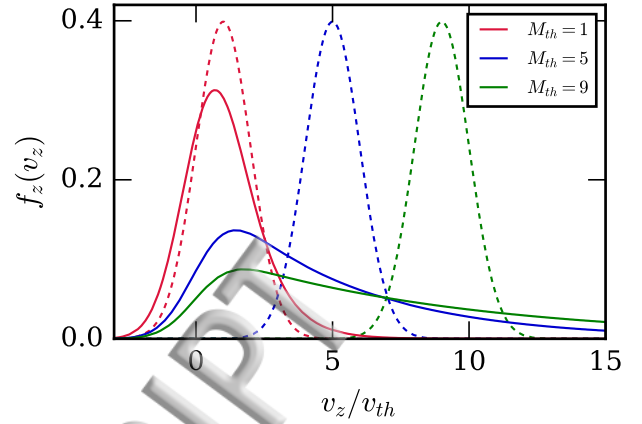


FIG. 1. Shift and drift velocity distribution function along the external field plotted versus velocity (normalized to the neutral thermal velocity) for three different thermal Mach numbers. The full lines depict the drift-driven distribution function [Eq. (1)] while the dashed lines represent the corresponding shifted Maxwellian distributions.

where $c_s = \sqrt{T_e/m_i}$ is the ion sound speed. To illustrate the two kinds of ion distributions, we present a comparison of the shifted Maxwellian distribution and the drift-driven distribution in Fig. 1. One can clearly see that the difference in the two distributions increases for higher thermal Mach numbers.

III. PARTICLE-IN-CELL SIMULATIONS

For our simulations, we have used the three-dimensional Cartesian mesh, oblique boundary, particles and thermals in cell (COPTIC) code²⁰. COPTIC is a hybrid particle-in-cell code in a sense that electron dynamics are governed by the Boltzmann description, $n_e = n_{e\infty} \exp(e\phi/T_e)$, whereas ion dynamics are considered in six-dimensional phase space in the presence of the self-consistent electric field and an optional external field.

The equation to delineate the ion dynamics in six-dimensional phase space in the presence of the self-consistent electric field $-\nabla\phi$ and an optional external force \mathbf{D} is²⁶

$$m_i \frac{d\mathbf{v}}{dt} = -e\nabla\phi + \mathbf{D}. \quad (2)$$

For the *shifted Maxwellian distribution*, this extra force \mathbf{D} is zero, and ions are driven solely by a flow of neutrals. On the other hand, for the *drift-driven distribution* (non-Maxwellian distribution), the neutrals are stationary, and the non-zero force field \mathbf{D} is responsible for the ion drift. The force \mathbf{D} thus represents the effect of the background electric field of Sec. II. However, it is not taken into account in the calculation of the electron

Boltzmann factor. This preferred choice leads to a uniform electron density in the absence of the dust grain, see also the discussion in Ref.²⁶.

While the simulations are performed in 3D Cartesian coordinates, the grain potential $\phi(r, z)$ has a cylindrical symmetry around the flow, which is here along the positive \hat{z} direction. In order to improve statistics, the full three-dimensional potential from the simulation is averaged over the cylindrical angle. The radial coordinate $r = \sqrt{x^2 + y^2}$ is limited by the box size and given by $\sqrt{2}l_b$, where l_b is the box half-width. For $r \gtrsim l_b$, the grain potential is increasingly affected by the finite box size.²⁹ In this work, the component of potential gradient along \hat{z} direction is set to be zero on the computational boundary. For the other two directions, the potential gradient is set to be zero in the $M\hat{z} + \hat{r}$ direction, where \hat{r} is the radial direction²⁹.

The simulation runs are performed with more than 30 million ions on a $64 \times 64 \times 128$ cell grid. Note that some figures have been obtained with finer grid resolution and non-uniform mesh spacing²⁰. Length scale, velocity and other normalizations are adopted from the paper by Hutchinson et al.²⁰, i.e., the space coordinate is normalized as $r \rightarrow r/r_0$, velocity as $v \rightarrow v/c_s$, and potential as $\phi \rightarrow \phi/(T_e/e)$, where $r_0 = (\lambda_{De}/5)$ is the normalizing scale length and c_s is unity in normalized units. The Debye length is fixed at $5r_0$ and the collision frequency ν is normalized in the time units as $\nu/(c_s/r_0) \sim 0.2(\nu/\omega_{pi})$, where ω_{pi} is the ion plasma frequency. The code is time-advanced for 1000 time-steps. We have summarized the simulation parameters in Table I.

In this work, we have considered only point-charge grains using the particle-particle-particle-mesh (PPPM) scheme³⁰ implemented in COPTIC²⁰. Here, the grain potential is treated analytically in a sphere of a predefined radius r_a around the grain shielded by opposite charge cloud²¹. The field due to the analytic potential is zero outside this predefined radius. The remaining potential is represented on the grid by solving the discrete Poisson equation. The advantage of this method is that the mesh does not have to resolve the grain potential near the grain where it is represented in analytic form, thus allowing for a coarser mesh without sacrificing accuracy^{20,21}. In this work, the analytical radius for point-charge sphere is chosen as $r_a = 0.1\lambda_{De}$.

Collisions are incorporated according to a Poisson statistical distribution with fixed velocity-independent collision frequency, i.e., the same assumption as is used in the derivation of Eq. (1) (BGK-type collisions). Charge-exchange collisions of ions with neutrals are performed by exchanging the velocity of the colliding ion with the velocity of a neutral chosen randomly from the (uniform) neutral velocity distribution²⁰. As we will see in sec. IV, collisions substantially alter the dynamics by changing the wakefield potential amplitude as well as the number of oscillations behind the grain.

TABLE I. Detailed list of the simulation parameters.

T_e/T_i	100
Mach Number, M	0.2 - 1.5
ν/ω_{pi}	0.002 - 2
λ_{De}	5
grid size	$64 \times 64 \times 128$
number of particles	30×10^6
total number of time steps	1000
ϕ_a	0.05-0.2
dt	0.1

IV. ANALYSIS OF THE WAKE POTENTIAL

We have performed a systematic study of the wake potential as a function of both, the Mach number and the collision frequency. The electron-ion temperature ratio was fixed at $T_e/T_i = 100$. To delineate the differences in the wake potential for the Maxwellian and non-Maxwellian distribution, we performed simulations for parameters in the range $M = v_d/c_s = 0.2 - 1.5$ and $\nu/\omega_{pi} = 0.002-2.0$.

A. Scaling with grain charge

The potential ϕ_a is equal to the potential of a point charge placed at the origin, i.e., $\phi_a = Q/(4\pi\epsilon_0 r_a)$. Writing the normalized charge \bar{Q} as

$$\bar{Q}_d = Q_d e / (4\pi\epsilon_0 \lambda_{De} T_e), \quad (3)$$

one obtains²¹

$$\bar{Q}_d = \phi_a / (T_e/e) \times (r_a / \lambda_{De}). \quad (4)$$

The effective charge \bar{Q}_d in the simulation is varied by varying the potential ϕ_a since $r_a/\lambda_{De} = 0.1$ is kept constant. Further, we have the relation between capacitance and charge for a small spherical object with radius r_p ($r_p/\lambda_{De} \ll 1$),

$$C = Q/\phi_p \approx 4\pi\epsilon_0 r_p. \quad (5)$$

Since OML theory predicts grain floating potentials as $\phi_p \approx -2T_e/e$ (ignoring the ion flow and collisions), the potential ϕ_a is representative of the effective grain radius²¹. Those ions which enter the grain radius are removed from the simulation²¹. Considering typical dusty plasma parameters, for an electron temperature of 2.585 eV and electron Debye length $\lambda_{De} = 845\mu\text{m}$, the grain charge is $Q_d = 1.51 \times 10^4 e$ for $\phi_a = -0.1T_e/e$.

Typical examples for the wake potential, as obtained from COPTIC, are shown in Fig. 2. The flow is in the positive \hat{z} direction. The potential shows one or several oscillations along the streaming direction, depending on the plasma conditions. By definition, in the linear

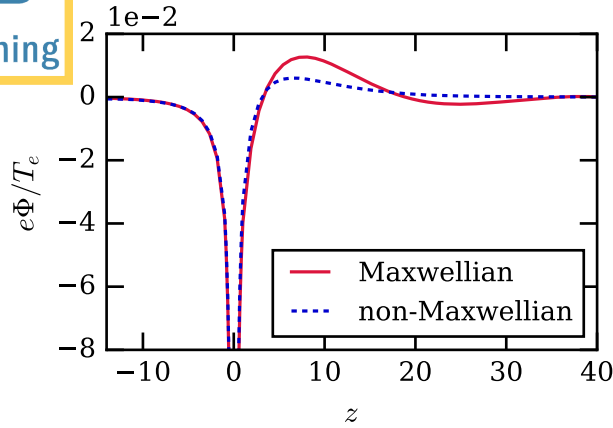


FIG. 2. Wake potential along the streaming axis for $M = 1$ ($M_{th} = 10$) and $\nu/\omega_{pi} = 0.02$. The solid (dashed) line corresponds to the shifted Maxwellian (non-Maxwellian) distribution.

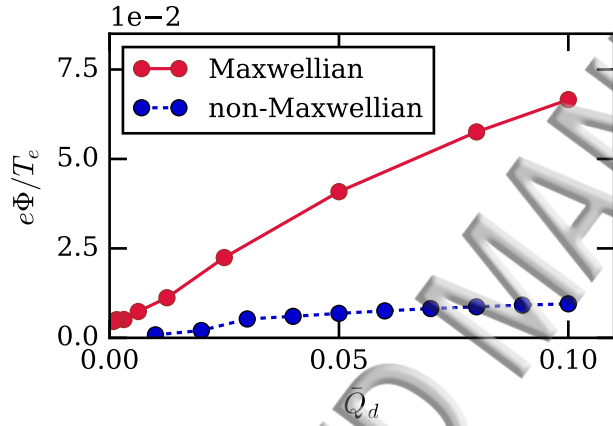


FIG. 3. Variation of the maximum of the wake potential with object charge in normalized units for the shifted Maxwellian distribution (solid line in red color) and the non-Maxwellian field-driven distribution (dashed line in blue color) at $M = 1$ ($M_{th} = 10$) and $\nu/\omega_{pi} = 0.2$.

regime, the potential $\Phi(\vec{r})$ is linearly proportional to the grain charge. In order to investigate the scaling behavior with PIC simulations, we varied the input grain charge (which is defined, in COPTIC, in terms of the grain potential, as discussed above) and calculated the height of the first potential peak.

The trend of the wake peak height with grain charge is shown in Fig. 3. To observe the relation between charge and maximum wake potential, we spanned a wide range of grain charge values and limit the following discussion to a maximum grain charge of $Q_d = 1.51 \times 10^5 e$ which is here equal to $\bar{Q}_d = 0.1$. Note that the amplitude of the peak, for the shifted Maxwellian distribution, is sig-

nificantly higher than for the non-Maxwellian case. This is due to the fact that ion focusing behind the grain is stronger in the shift case than in the drift case. This behavior is found for very small charge on the dust also. Note, however that, for very small grain charges, the determination of the exact wake peak potential is difficult due to numerical limitations.

Nonlinear effects should be particularly important for slow ions whose kinetic energy is insufficient to escape from the potential well created by the dust grain. From Fig. 1 it is evident that, in the Maxwellian case, the number of low-velocity ions is very low in the shifted Maxwellian case while in the non-Maxwellian distribution an appreciable fraction of low velocity ions remains even for $M_{th} \approx 10$.

Our goal here is to study the role of collisions on the wake potential. To study the wake behavior, we limit the following discussion to the normalized grain charge $\bar{Q}_d = 0.01$ in order to minimize the non-linear effects without sacrificing computational accuracy.

B. Influence of collisionality

Figure 4 shows the qualitatively similar physical roles played by collisional and collisionless damping for the topology of the potential. The vertical dashed lines in the contour plot denote the half-width of the box beyond which the region is subject to distortion due to the boundary. Maxwellian ions with low ion-neutral damping lead to pronounced oscillations of the wake potential in the streaming direction, which is well known from linear response calculations^{16,18} and PIC simulations^{18,20,31,32}. However, these oscillations are almost completely absent in the case of non-Maxwellian ions²⁶. As can be seen from Fig. 4, this effect on the wake potential can be closely mimicked in the Maxwellian case by increasing the ion-neutral collision frequency. Even though the damping mechanisms are very different, the eventual effect on the wake oscillations is the same and clearly visible.

We now investigate the influence of ion-neutral collisions in greater detail. In Fig. 5, we present wake potential contours, for various collision frequencies, for the shifted Maxwellian distribution. Similar to observations made in linear response calculations¹⁸, here we also observe that the role of collisions is to reduce and damp the wake oscillations behind the grain, for moderate to high Mach numbers²⁹. Figure 6 depicts the same results but now for the non-Maxwellian drift-driven distribution. As observed by Hutchinson *et al.*²⁶ and in Fig. 4, the wakes are strongly damped, and only one positive peak behind the grain remains. Unlike in the shifted Maxwellian case, there are no trailing oscillations behind the grain. As we increase the collisionality from $\nu/\omega_{pi} = 0.02$ to $\nu/\omega_{pi} = 0.4$, we have increased noise due to the injection of ions in the highly collisional regime, which is visible as a potential maximum upstream of the grain. We have performed rigorous convergence tests w.r.t. the number

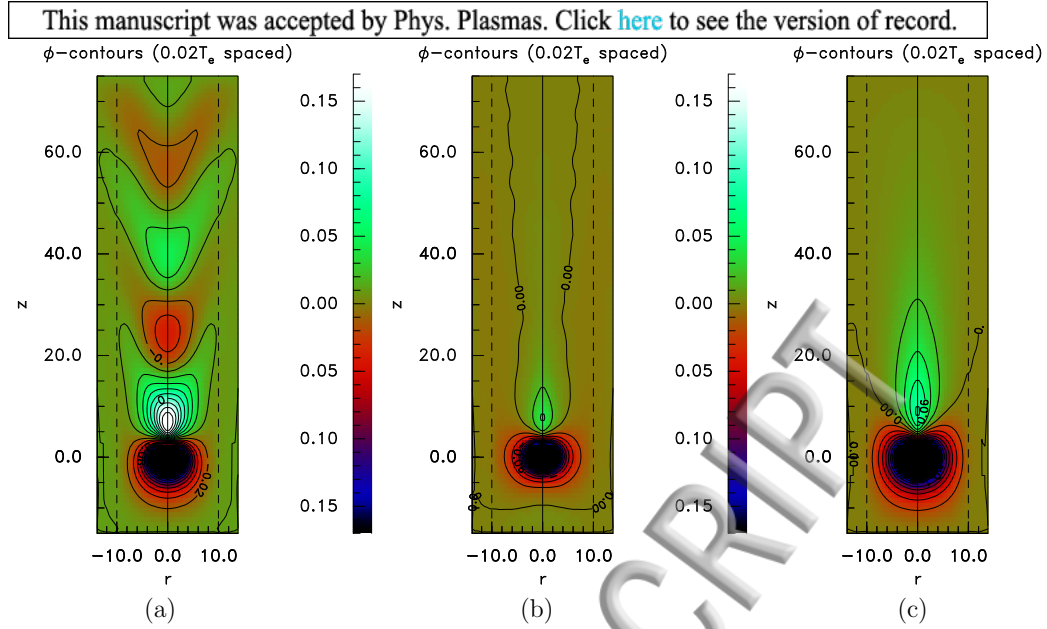


FIG. 4. Wake potential contours $e\phi/T_e$, averaged over the azimuthal angle, for (a) the shifted Maxwellian distribution (almost collisionless, $\nu/\omega_{pi} = 0.001$); (b) the field-driven non-Maxwellian distribution ($\nu/\omega_{pi} = 0.001$) and (c) the shifted Maxwellian with collisions ($\nu/\omega_{pi} = 0.5$). The Mach number is identical ($M = 1$) in all cases. Here, the grain is at the origin and the normalized grain charge is $\bar{Q}_d = 0.02$.

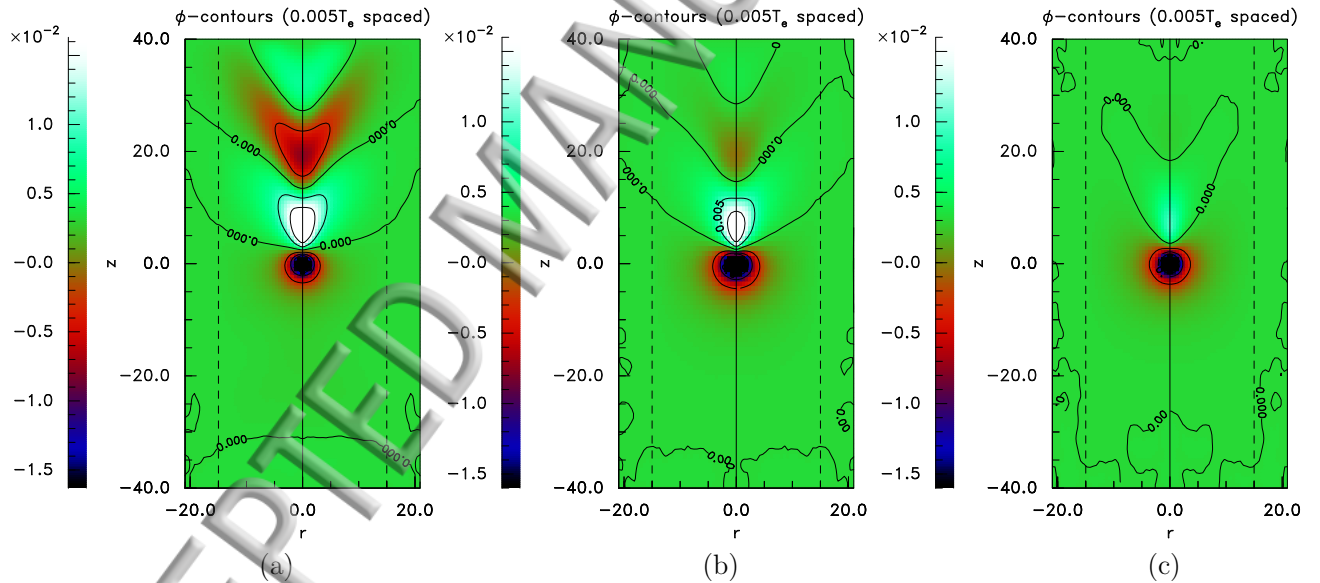


FIG. 5. Contour plots of the grain potential $e\phi/T_e$ for various collision frequencies: (a) $\nu/\omega_{pi} = 0.02$; (b) $\nu/\omega_{pi} = 0.2$, and (c) $\nu/\omega_{pi} = 0.4$ with streaming velocity $M = 0.8$ for the shifted Maxwellian case. Here, the grain is at the origin and the normalized grain charge is $\bar{Q}_d = 0.01$.

of particles as well as the box size to avoid boundary effects on the wake potential.

At higher collisionality, there is an appreciable fraction of slow ions which eventually lose their energy due to collisions. These slow moving ions cannot escape the potential well and become trapped. The density of these trapped ions builds up over time, and they contribute to the enhancement of the peak amplitude with increased

collisionality³⁶. A similar discussion with regard to the calculation of drag forces on the grain can be found in Ref.²⁶.

The variations of the maximum peak height and the peak position with collisionality, for Maxwellian as well as non-Maxwellian ions, are shown in Fig. 7. First, we consider the regime of slow streaming velocity, $M = 0.2$, cf. Fig. 7 (left column). Collision-induced amplification

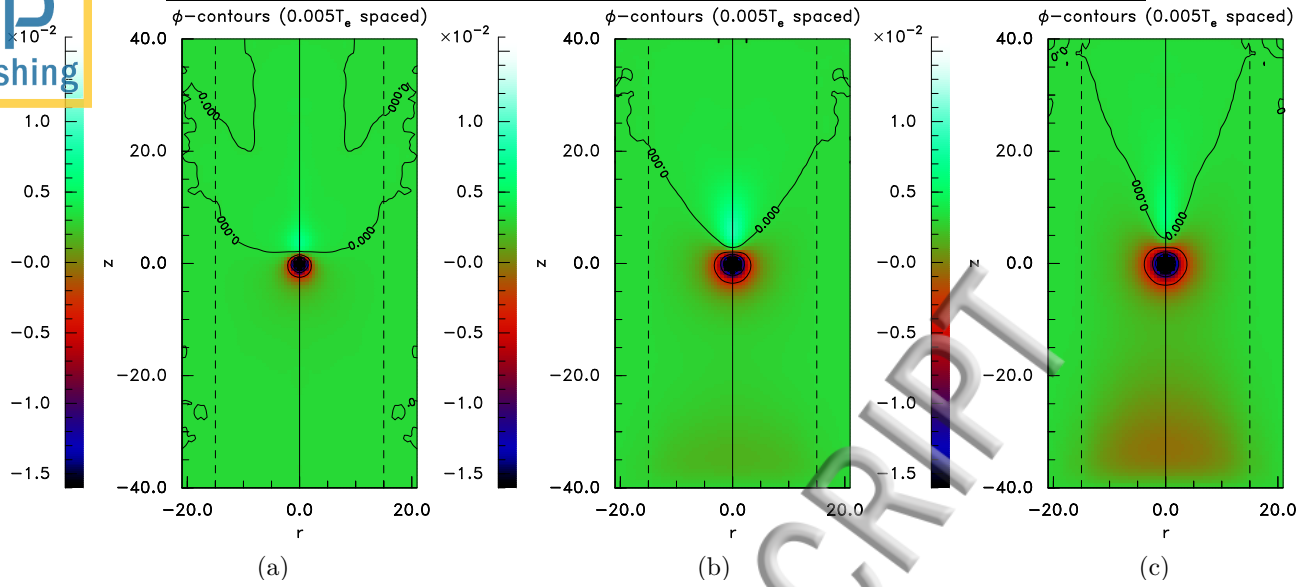


FIG. 6. Contour plots of the grain potential $e\phi/T_e$, for various collision frequencies: (a) $\nu/\omega_{pi} = 0.02$; (b) $\nu/\omega_{pi} = 0.2$, and (c) $\nu/\omega_{pi} = 0.4$ with streaming velocity $M = 0.8$ for the non-Maxwellian case. Here, the grain is at the origin and the normalized grain charge is $\bar{Q}_d = 0.01$.

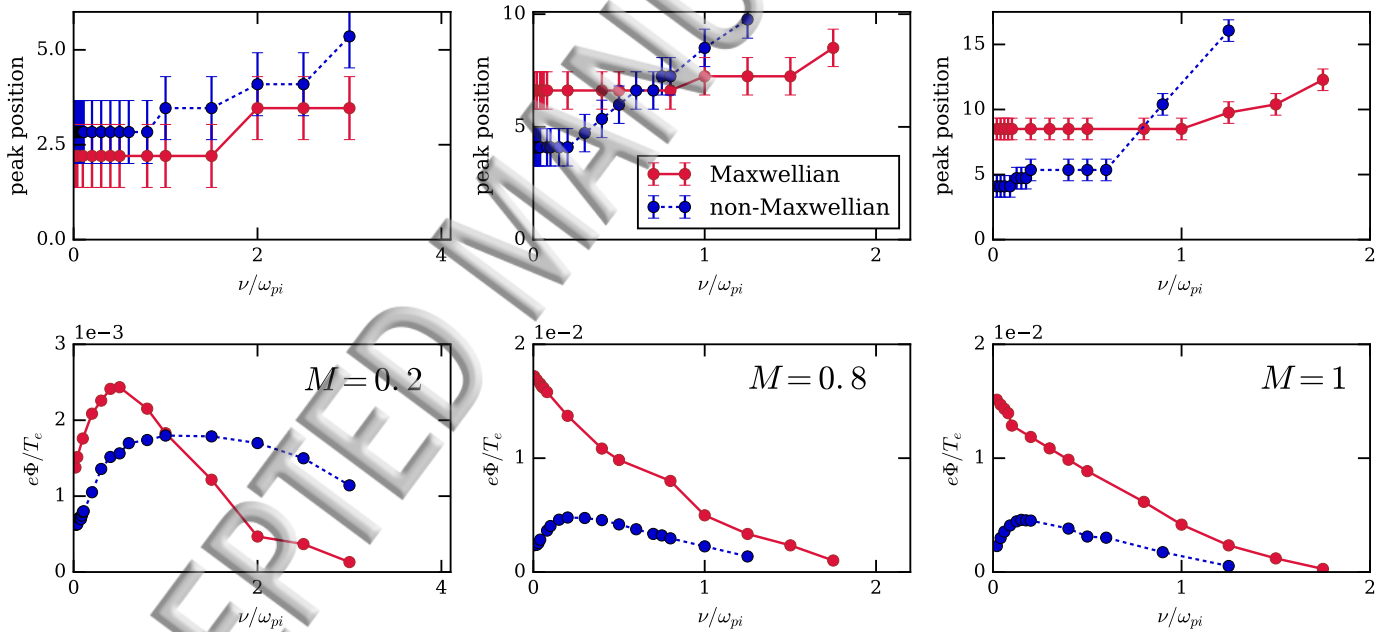


FIG. 7. Peak position (top row) and peak amplitudes (bottom row) of the wake potential as a function of collision frequency for shifted Maxwellian (solid) and non-Maxwellian (dashed) drift-driven distributions for $T_e/T_i = 100$ and $M = 0.2, 0.8, 1$ for $\bar{Q}_d = 0.01$.

is noticed here for the non-Maxwellian distribution with a significant increase by a factor 3 from $\nu/\omega_{pi} = 0.01$ to $\nu/\omega_{pi} \sim 0.8$. For larger ν/ω_{pi} , we observe a drop of the peak height, indicating a broad maximum around $\nu/\omega_{pi} \sim 0.8 - 1.5$. The peak position is almost constant up to $\nu/\omega_{pi} \sim 0.8$ but starts increasing with increasing

collisionality. For the shifted Maxwellian case also, we observe collision-induced amplification up to $\nu/\omega_{pi} \sim 0.5$. However, the maximum is much more narrow, and the wake amplitude strongly decreases for $\nu/\omega_{pi} \gtrsim 0.5$. The peak position is slightly shifted towards the grain when compared with the non-Maxwellian case. It should be

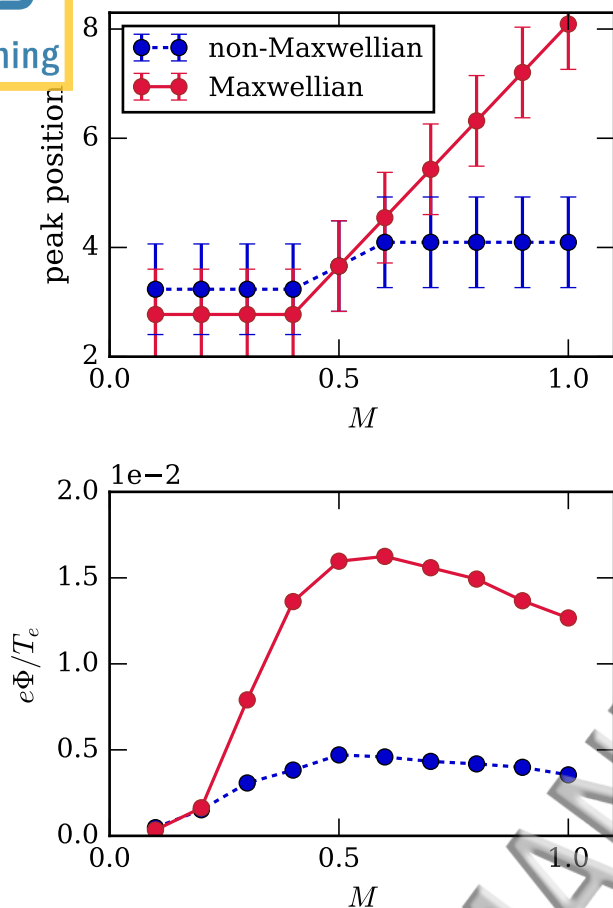


FIG. 8. Peak position (top) and peak amplitude (bottom) of the wake potential in normalized units for $T_e/T_i = 100$ as a function of Mach number, for a shifted Maxwellian (solid) and a non-Maxwellian (dashed) drift-driven distribution, for the collision frequency $\nu/\omega_{pi} = 0.2$ and $Q_d = 0.01$.

noted that at higher collisionality, numerical noise is high which puts a constraint on the simulations. [Grid resolution puts a limitation on the precision up to which one can accurately determine the value of peak position.](#)

In Figure 7 (middle column), we present the variations of the maximum peak height and the peak position with collisionality, for the higher flow velocity, $M = 0.8$. As in the case $M = 0.2$ we observe collision-induced amplification for small collisionality, $\nu/\omega_{pi} \lesssim 0.3$, for the non-Maxwellian distribution. When the collisionality increases further, the peak amplitude begins to show a slow decline. The peak position is constant only for very small collisionality (up to $\nu/\omega_{pi} = 0.2$) and increases beyond that collisionality. On the other hand, for the shifted Maxwellian case, damping of the peak potential amplitude is observed¹⁸ with increase in collisionality. The peak position is almost constant up to $\nu/\omega_{pi} \sim 0.8$ but starts increasing slightly, at higher collisionality.

For $M = 1$, the peak positions (top right figure) re-

main constant (within the grid resolution) over a broad range of collision frequencies (up to $\nu/\omega_{pi} = 1$) considered here, for Maxwellian distribution and exhibits a rapid increase in peak position for non-Maxwellian distribution. For a non-Maxwellian distribution, the peak is substantially closer to the dust grain, compared to the shifted Maxwellian case for smaller collisionality. Consider now the peak height (bottom right figure). While an increase in collisionality from the collisionless case to $\nu/\omega_{pi} = 0.4$ decreases the height, for the shift distribution, we find that the amplitude for the drift distribution increases significantly, by a factor ~ 3 . The trend of wake potential peak and position at higher streaming speeds (i.e. $M = 1$ and $M = 0.8$) is qualitatively similar but differs significantly from small streaming speed $M = 0.2$.

We observe a decrease of the peak height (as in the case $M = 0.8$) for Mach number larger than 0.4 for shifted Maxwellian distribution in contrast to non-Maxwellian, whereas for smaller values of streaming speed the peak potential height exhibits a non-monotonic behavior with collisionality for both Maxwellian as well as non-Maxwellian distribution but for different values of ν/ω_{pi} (see left column of Fig. 7 for $M = 0.2$). The qualitative behavior of peak potential amplitude is similar for both the distributions at very small streaming speeds (i.e. $M = 0.2$). These results are in agreement with the data presented by Hutchinson²⁹ (see, in particular, figure 2 in²⁹). [We note that the difference in consecutive values of the peak positions and the peak height is due to the constraint on the grid resolution.](#)

This peculiar behavior of the wake pattern for the two different distributions²⁶ can be understood as follows. In the shifted Maxwellian case, after an ion-neutral charge-exchange collision, the new ion is born with an average velocity equal to the flow velocity. For higher Mach numbers, irrespective of collisionality, fast ions have enough energy to overcome the potential barrier and reduce the ion shielding near the grain, which eventually results in an enhanced shielding length. This is why we do not observe any collision induced amplification of the wake for higher flow velocities in the shifted Maxwellian case. On the other hand, in the drift case, an ion that has undergone a collision, is “reborn” with zero average velocity. In order to leave the potential well, the ion must first gain a sufficient amount of kinetic energy. At subsonic flow velocities, the behavior is similar to the shifted Maxwellian case. Here also, we see collision-induced amplification of the wake. However, at higher flow velocities, the features are altogether different. At higher flow speeds, the drift-driven non-Maxwellian distribution contains a large fraction of streaming ions in the subsonic range. These subsonic flow ions contribute to shielding and enhancement of the wake amplitude with collision. Thus, collisions lead to an amplification of the maximum wake amplitude, even for high Mach numbers, for a non-Maxwellian distribution.

In Fig. 8, we present the magnitude of the potential peak position and peak height as a function of Mach

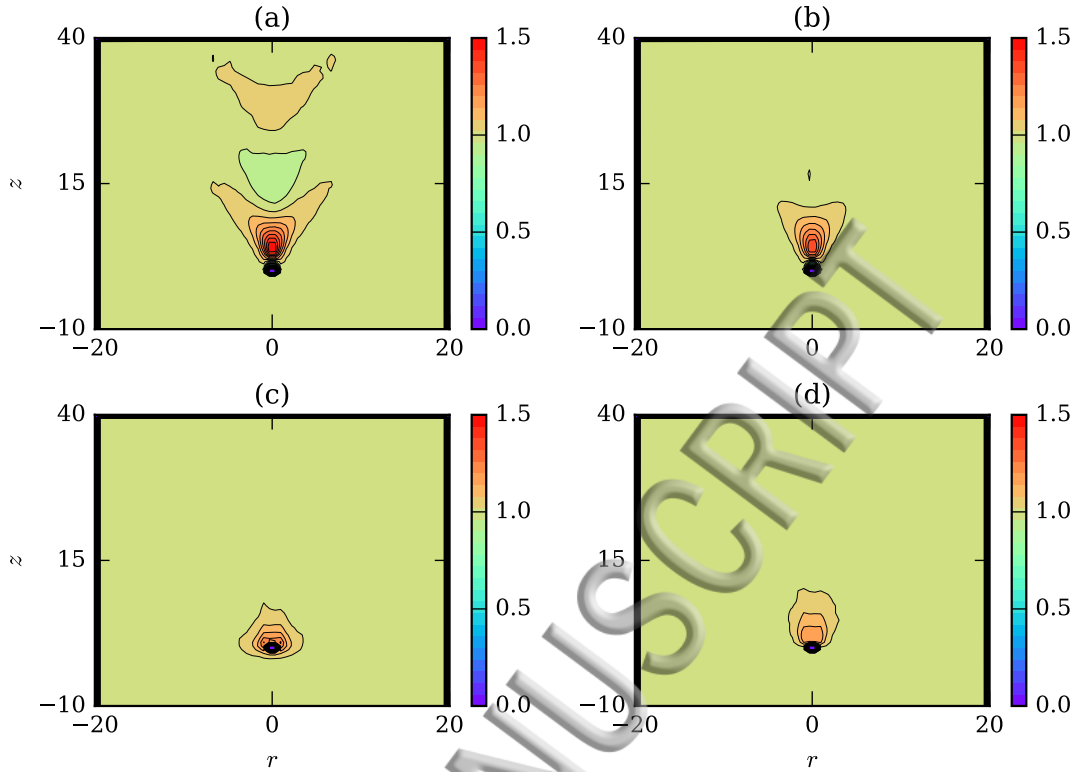


FIG. 9. Spatial profiles of the ion density (normalized to the distant unperturbed ion density), for a Mach number $M = 0.8$, for a shifted Maxwellian (top row) and a non-Maxwellian drift distribution (bottom row), for a collision frequency of $\nu/\omega_{pi} = 0.02$ (left column) and $\nu/\omega_{pi} = 0.2$ (right column). Spatial scales r and z axes are in normalized units ($\lambda_{De}/5$).

number M . The wake potential amplitude versus Mach number plot has a non-monotonic behavior and reveals a maximum with the Mach number¹⁸. The amplitude of the wake potential initially increases, with an increase of the streaming velocity. At moderate velocities it starts to saturate. Here, we also observe a non-monotonic behavior of the peak potential with the Mach number. The overall peak amplitude of the wake is higher, for the shifted Maxwellian distribution. The peak position for non-Maxwellian is constant for smaller streaming speeds and shows a jump at $M = 0.6$ and then remains constant for higher streaming speeds. On the other hand, peak position for the non-Maxwellian case is constant for smaller streaming speeds but exhibits a monotonic increase with increasing ion flow velocity. The plot of wake potential vs flow speed compares fair with previous numerical work^{16,18}.

The distinctions between the shift and drift distribution cases can also be elucidated clearly with the density profiles for the two cases. In Figure 9 subplots (a) and (b), we present the density profile for two different collision frequencies ($\nu/\omega_{pi} = 0.02, 0.2$), in the Maxwellian case. The density contours also show a wake pattern similar to the potential wake (for $\nu/\omega_{pi} = 0.02$). With increasing collisionality, the peak of the density decreases

which is in agreement with the potential profiles. For lower collisionality, there is a large fraction of streaming ions that overcome the potential barrier and assist in wake formation, whereas at higher collisionality the number of fast ion accumulation is reduced slightly. For $\nu/\omega_{pi} = 0.2$, the ion focusing does not produce a wake pattern, rather there is big zero density region around the grain. The shielding of ions around the grain can be observed in the upstream direction as well.

In subplots (c) and (d) of Figure 9, we present the density profile for two different collision frequencies ($\nu/\omega_{pi} = 0.02, 0.2$) for the drift-driven non-Maxwellian distribution. Here, with increase in collisionality, the peak of the density increases, in contrast to the shifted Maxwellian case. In accordance to the corresponding potential profiles, here we do not observe ion density variations behind the grain. Moreover, slow ions create ion shielding around the grain, an effect that is missing for the shifted Maxwellian distribution²⁶.

V. SUMMARY AND DISCUSSIONS

In the present work, we have investigated the electrostatic potential distribution around a point-like charged

grain in a streaming plasma for a Maxwellian as well as for a non-Maxwellian ion distribution function, for a wide range of ion-neutral collision frequencies and Mach numbers. We have presented a comparative study of both cases, using accurate 3D particle-in-cell simulations.

The simulations are based on certain assumptions, i.e., we have ignored the role of plasma inhomogeneity, secondary electron emission, etc., which could be of importance for experimental systems. Nevertheless, we provide here an improved numerical work by including the effect of an external electric field and collisions on the wake potential and ion density. The electric field mimics the conditions encountered in real discharges, where the sheath electric field accelerates the ions towards the electrodes. Its effect has been neglected in many previous works, e.g., Refs.^{16,18,20}, but has received increasing attention in recent years, e.g.,^{22,25–28}. Compared to a situation where the ion flow is caused by a flow of neutrals, which gives rise to a shifted Maxwellian ion distribution, the inclusion of an external electric field yields a non-Maxwellian drift distribution. The high population of low-velocity ions, which persists even for high Mach numbers, strongly modifies the wake potential and the accumulation of the ions behind the dust grain.

In agreement with earlier simulations²⁶, our results show that in the non-Maxwellian case only a single potential maximum remains, even for weak ion-neutral damping. The higher order potential extrema found in linear response calculations^{16,18} and simulations²⁰ with a shifted Maxwellian distribution disappear. An important observation is collision-induced amplification of the wake potential. For the entire flow range considered in this paper, we find collision-induced amplification of the wake potential for the non-Maxwellian distribution. As the ion-neutral collision frequency is increased, the wake amplitude initially becomes significantly larger than in the collisionless limit. Upon further increase, it reaches a maximum and finally decreases. The location of the maximum was found to depend on the Mach number. On the other hand, in the case of a shifted Maxwellian ion distribution, we observe a maximum only for low streaming velocities ($M = 0.2$). For higher streaming velocities ($M = 0.8$ and $M = 1$), the wake amplitude was found to decrease monotonically with the collisionality.

Particle attraction caused by ion focusing has been reported in many experiments, e.g.,^{33,34,37,38}. In order to verify the collision-induced amplification of the wake potential experimentally, the ion-neutral collision rate must be sufficiently small. Our simulations show that only in this regime, an increase of the collisionality leads to amplification of the wake. The constraints on the ion Mach number are less severe since the effect occurs over a wide range. Nevertheless, it should be most pronounced for small M . Thus, the particle would ideally be located in a region with subsonic ion flow, i.e., in the presheath.

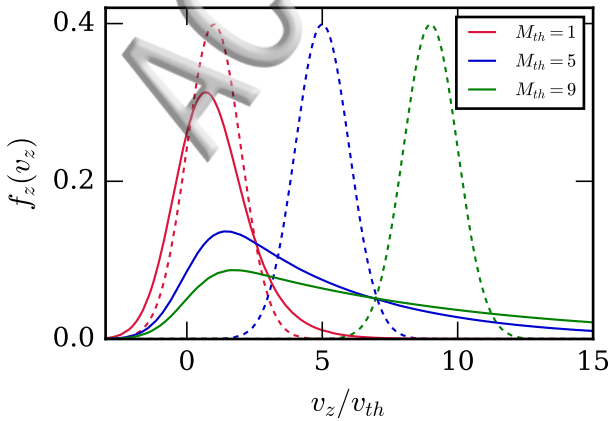
VI. ACKNOWLEDGMENTS

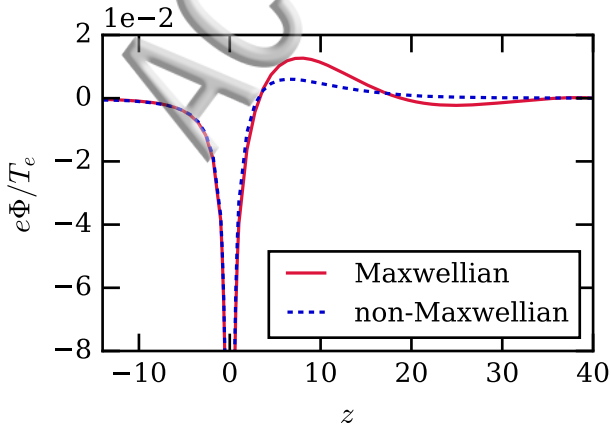
S. Sundar would like to thank I.H. Hutchinson for support in using the COPTIC code, and acknowledges support of CAU Kiel. This work was supported by the DFG via SFB-TR24, project A9. Our numerical simulations were performed at the HPC cluster of Christian-Albrechts-Universität zu Kiel.

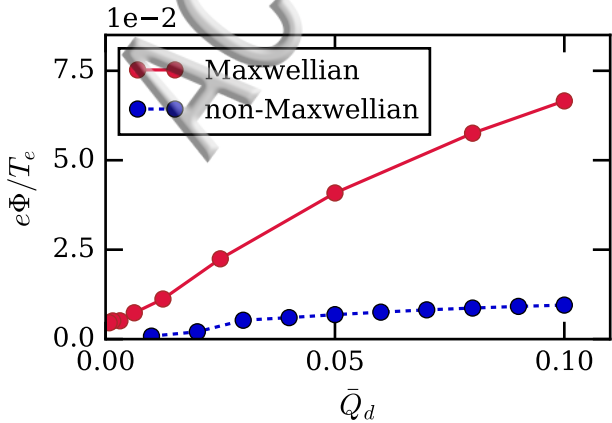
- ¹G. E. Morfill and A. V. Ivlev, “Complex plasmas: An interdisciplinary research field,” *Rev. Mod. Phys.* **81**, 1353–1404 (2009).
- ²A. Melzer and J. Goree, “Fundamentals of dusty plasmas,” *Low Temperature Plasmas* vol 1 Ed. R Hippler, H Kersten, M Schmidt and KH Schoenbach (2008).
- ³M. Bonitz, N. J. Horing, and P. Ludwig, eds., *Introduction to Complex Plasmas* (Springer, 2010).
- ⁴M. Bonitz, C. Henning, and D. Block, “Complex plasmas: a laboratory for strong correlations,” *Rep. Progress Phys.* **73**, 066501 (2010).
- ⁵J. H. Chu and L. I., “Direct observation of coulomb crystals and liquids in strongly coupled rf dusty plasmas,” *Phys. Rev. Lett.* **72**, 4009–4012 (1994).
- ⁶A. Barkan, R. L. Merlino, and N. D’angelo, “Laboratory observation of the dust-acoustic wave mode,” *Physics of Plasmas* **2**, 3563–3565 (1995).
- ⁷M. Kretschmer, S. A. Khrapak, S. K. Zhdanov, H. M. Thomas, G. E. Morfill, V. E. Fortov, A. M. Lipaev, V. I. Molotkov, A. I. Ivanov, and M. V. Turin, “Force field inside the void in complex plasmas under microgravity conditions,” *Phys. Rev. E* **71**, 056401 (2005).
- ⁸S. Barbosa, L. Coudel, C. Arnas, K. K. Kumar, C. Pardanaud, and F. R. A. Onofri, “In-situ characterisation of the dynamics of a growing dust particle cloud in a direct-current argon glow discharge,” *Journal of Physics D: Applied Physics* **49**, 045203 (2016).
- ⁹J. Winter, “Dust in fusion devices a multi-faceted problem connecting high- and low-temperature plasma physics,” *Plasma Physics and Controlled Fusion* **46**, B583 (2004).
- ¹⁰J. Sharpe, D. Petti, and H.-W. Bartels, “A review of dust in fusion devices: Implications for safety and operational performance,” *Fusion Engineering and Design* **6364**, 153 – 163 (2002).
- ¹¹S. Ratynskaia, C. Castaldo, E. Giovannozzi, D. Rudakov, G. Morfill, M. Horanyi, J. H. Yu, and G. Maddaluno, “In situ dust detection in fusion devices,” *Plasma Physics and Controlled Fusion* **50**, 124046 (2008).
- ¹²M. D. F. Graziani, R. Redmer, and S. Trickey, eds., *Frontiers and Challenges in Warm Dense Matter* (Springer, 2014).
- ¹³Z. Moldabekov, T. Schoof, P. Ludwig, M. Bonitz, and T. Ramazanov, “Statically screened ion potential and bohm potential in a quantum plasma,” *Physics of Plasmas* **22**, 102104 (2015), <http://dx.doi.org/10.1063/1.4932051>.
- ¹⁴P. Hartmann, Z. Donkó, G. J. Kalman, S. Kyrkos, K. I. Golden, and M. Rosenberg, “Collective dynamics of complex plasma bilayers,” *Phys. Rev. Lett.* **103**, 245002 (2009).
- ¹⁵P. Hartmann, A. Douglass, J. C. Reyes, L. S. Matthews, T. W. Hyde, A. Kovács, and Z. Donkó, “Crystallization dynamics of a single layer complex plasma,” *Phys. Rev. Lett.* **105**, 115004 (2010).
- ¹⁶M. Lampe, G. Joyce, G. Ganguli, and V. Gavrishchaka, “Interactions between dust grains in a dusty plasma,” *Physics of Plasmas* **7**, 3851–3861 (2000).
- ¹⁷D. Winske, “Nonlinear wake potential in a dusty plasma,” *IEEE Transactions on Plasma Science* **29**, 191–197 (2001).
- ¹⁸P. Ludwig, W. J. Miloch, H. Kählert, and M. Bonitz, “On the wake structure in streaming complex plasmas,” *New Journal of Physics* **14**, 053016 (2012).
- ¹⁹D. Block, J. Carstensen, P. Ludwig, W. Miloch, F. Greiner, A. Piel, M. Bonitz, and A. Melzer, “Wake formation and

- wake field effects in complex plasmas," *Contributions to Plasma Physics* **52**, 804–812 (2012).
- ²⁰I. H. Hutchinson, "Nonlinear collisionless plasma wakes of small particles," *Physics of Plasmas* **18**, 032111 (2011).
- ²¹I. H. Hutchinson, *Plasma Physics and Controlled Fusion* **55**, 115014 (2013).
- ²²M. Lampe, T. B. Röcker, G. Joyce, S. K. Zhdanov, A. V. Ivlev, and G. E. Morfill, "Ion distribution function in a plasma with uniform electric field," *Physics of Plasmas* **19**, 113703 (2012).
- ²³A. V. Ivlev, S. K. Zhdanov, S. A. Khrapak, and G. E. Morfill, "Kinetic approach for the ion drag force in a collisional plasma," *Phys. Rev. E* **71**, 016405 (2005).
- ²⁴L. Patacchini and I. H. Hutchinson, "Fully self-consistent ion-drag-force calculations for dust in collisional plasmas with an external electric field," *Phys. Rev. Lett.* **101**, 025001 (2008).
- ²⁵H. Kählert, "Ion-dust streaming instability with non-maxwellian ions," *Physics of Plasmas* **22**, 073703 (2015).
- ²⁶I. H. Hutchinson and C. B. Haakonsen, "Collisional effects on nonlinear ion drag force for small grains," *Physics of Plasmas* **20**, 083701 (2013).
- ²⁷R. Kompaneets, G. E. Morfill, and A. V. Ivlev, "Interparticle attraction in 2d complex plasmas," *Phys. Rev. Lett.* **116**, 125001 (2016).
- ²⁸R. Kompaneets, G. E. Morfill, and A. V. Ivlev, "Wakes in complex plasmas: A self-consistent kinetic theory," *Phys. Rev. E* **93**, 063201 (2016).
- ²⁹I. H. Hutchinson, "Intergrain forces in low-mach-number plasma wakes," *Phys. Rev. E* **85**, 066409 (2012).
- ³⁰R. W. Hockney and E. J. W., "Computer simulation using particles," Taylor and Francis, London (1988).
- ³¹W. J. Miloch, "Wake effects and mach cones behind objects," *Plasma Physics and Controlled Fusion* **52**, 124004 (2010).
- ³²W. J. Miloch, M. Kroll, and D. Block, "Charging and dynamics of a dust grain in the wake of another grain in flowing plasmas," *Physics of Plasmas* **17**, 103703 (2010), <http://dx.doi.org/10.1063/1.3488252>.
- ³³A. Melzer and A. Schella, *Phys. Rev. E* **89**, 041103 (2014).
- ³⁴M. Kroll, J. Schablinski, D. Block, and A. Piel, *Physics of Plasmas* **17**, 013702 (2010).
- ³⁵I. H. Hutchinson, arXiv preprint arXiv:1105.1356 (2011).
- ³⁶M. Lampe, R. Goswami, Z. Sternovsky, S. Robertson, V. Gavriishchaka, G. Ganguli, and G. Joyce, "Trapped ion effect on shielding, current flow, and charging of a small object in a plasma," *Physics of Plasmas* **10**, 1500–1513 (2003).
- ³⁷H. Jung, F. Greiner, O. H. Asnaz, J. Carstensen, and A. Piel, "Exploring the wake of a dust particle by a continuously approaching test grain," *Physics of Plasmas* **22**, 053702 (2015).
- ³⁸G. A. Hebner, M. E. Riley, and B. M. Marder, "Attractive interactions between negatively charged dust particles levitated at the plasma-sheath boundary layer," *IEEE Transactions on Plasma Science* **33**, 396–397 (2005).

ACCEPTED MANUSCRIPT

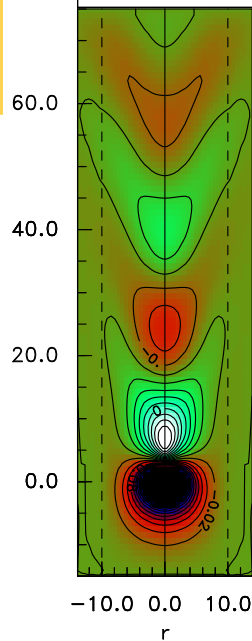
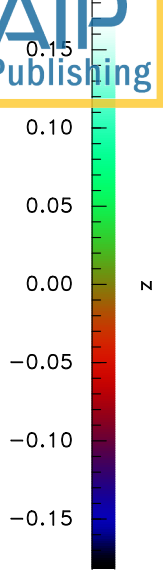




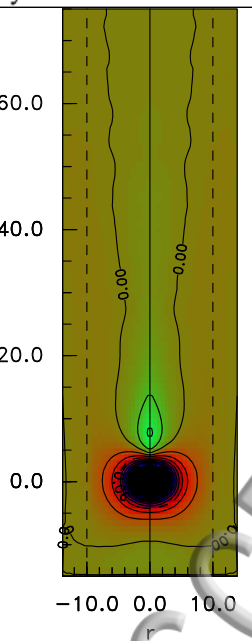
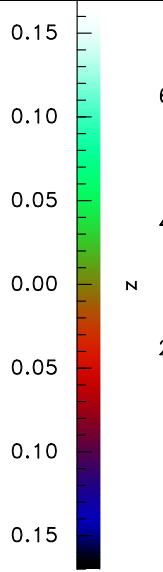




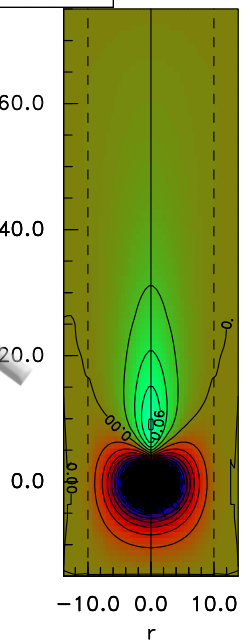
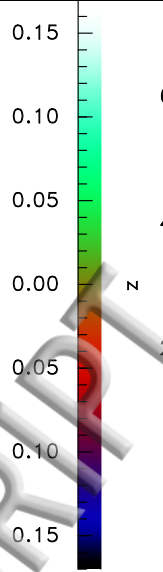
ϕ -contours (0.02T_e spaced) This manuscript was accepted by Phys. Plasmas. Click [here](#) to see the version of record. ϕ -contours (0.02T_e spaced) ϕ -contours (0.02T_e spaced)



(a)



(b)

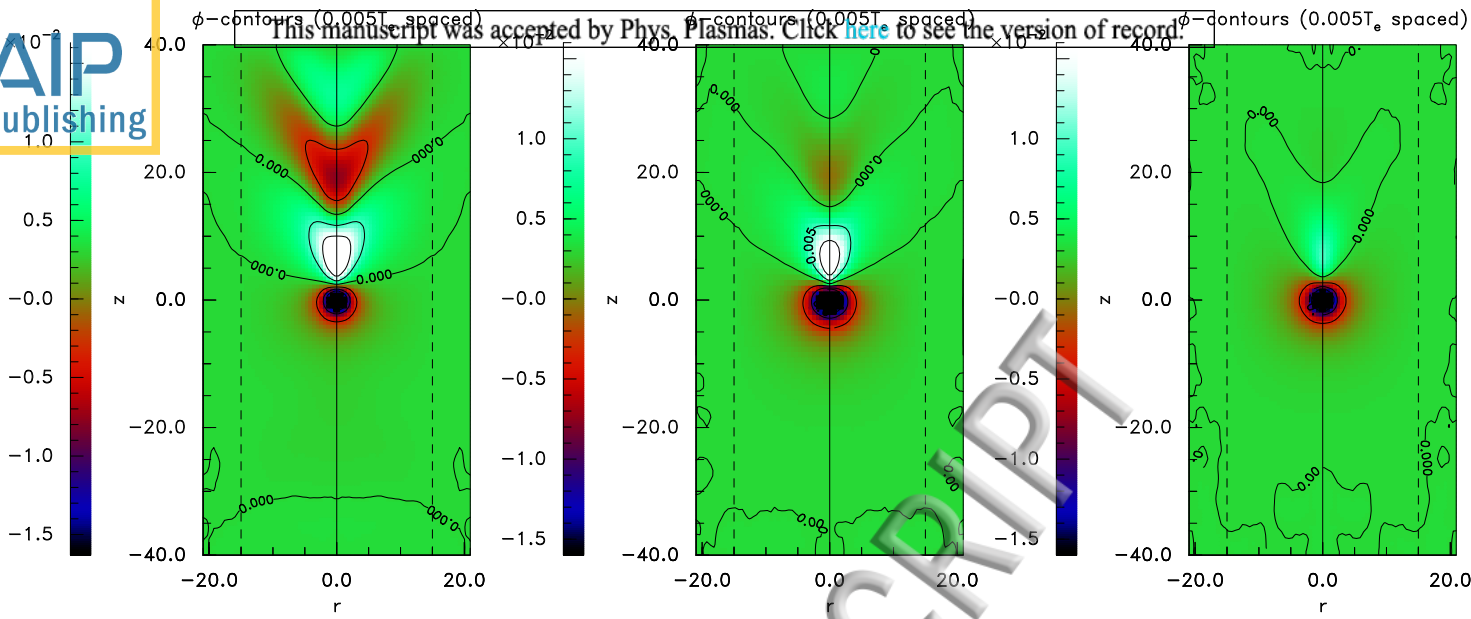


(c)

ACCEPTED MANUSCRIPT



This manuscript was accepted by Phys. Plasmas. Click here to see the version of record.

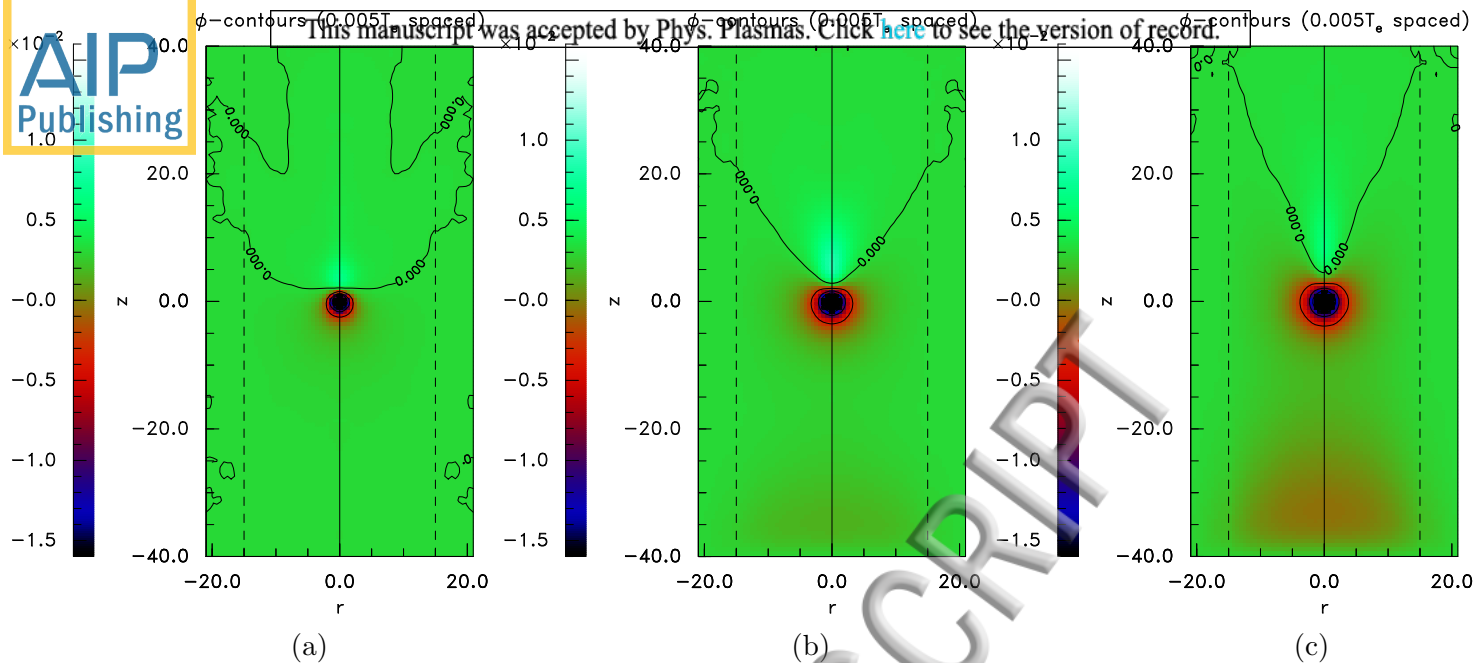


(a)

(b)

(c)

ACCEPTED MANUSCRIPT



ACCEPTED MANUSCRIPT

